

Identification of a Putative Binding Site for [2',5'-Bis-*O*-(*tert*-butyldimethylsilyl)- β -D-ribofuranosyl]-3'-spiro-5''-(4''-amino-1'',2''-oxathiole-2'',2''-dioxide)thymine (TSAO) Derivatives at the p51–p66 Interface of HIV-1 Reverse Transcriptase

Fátima Rodríguez-Barrios,[†] Carlos Pérez,[†] Esther Lobatón,[‡] Sonsoles Velázquez,[‡] Cristina Chamorro,[‡] Ana San-Félix,[‡] María-Jesús Pérez-Pérez,[‡] María-José Camarasa,[‡] Heidi Pelemans,[§] Jan Balzarini,[§] and Federico Gago^{*,†}

Departamento de Farmacología, Universidad de Alcalá, E-28871 Alcalá de Henares, Madrid, Spain, Instituto de Química Médica, CSIC, c/Juan de la Cierva 3, E-28006 Madrid, Spain, and Rega Institute for Medical Research, Katholieke Universiteit Leuven, B-3000 Leuven, Belgium

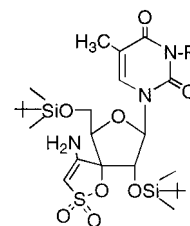
Received October 10, 2000

A binding site for TSAO-m³T at the interface between the p66 and p51 subunits of HIV-1 reverse transcriptase (RT) and distinct from that of “classical” HIV-1 non-nucleoside inhibitors is proposed. The feasibility of the binding mode was assessed by carrying out nanosecond molecular dynamics simulations for the complexes of TSAO-m³T with reduced models of both the wild-type enzyme and a more sensitive R172A mutant. The molecular model is in agreement with a previous proposal, with known structure–activity and mutagenesis data for this unique class of inhibitors, and also with recent biochemical evidence indicating that TSAO analogues can affect enzyme dimerization. The relative importance of residues involved in dimer formation and TSAO–RT complex stabilization was assessed by a combination of surface area accessibility, molecular mechanics, and continuum electrostatics calculations. A structure-based modification introduced into the lead compound yielded a new derivative with improved antiviral activity.

Introduction

Human immunodeficiency virus type 1 (HIV-1) reverse transcriptase (RT) is composed of a 560-residue subunit (p66) and a 440-residue subunit (p51), which together catalyze both RNA-dependent and DNA-dependent DNA polymerization reactions.¹ Crystal structures of unliganded RT,² RT–DNA complexes,³ and RT–inhibitor complexes⁴ have consistently shown that, despite the amino acid identity in both subunits, the polymerase subdomains (called fingers, palm, thumb, and connection) are arranged differently in each one, with p66 forming a large active site cleft and p51 forming an inactive closed structure⁵ that provides structural support to the polymerase domain of p66.^{6,7} For the process of native dimerization, a two-step model has been proposed in which the dimers are in equilibrium with the folded inactive monomers.⁸ The first step is a concentration-dependent association of p66 and p51 that yields an intermediate that slowly isomerizes to the “mature” heterodimeric form of the enzyme.⁹

Two classes of RT inhibitors are in clinical use: nucleoside analogues that, upon metabolic activation, bind to the polymerase active site and non-nucleoside inhibitors (NNRTIs) that lock RT into an inactive conformation by fitting into an allosteric site near to, but distinct from, the polymerase active site.¹⁰ Despite current advances in combination therapy,¹¹ numerous mutations are known that confer resistance to both



R = H TSAO-T (1)
R = CH₃ TSAO-m³T
R = CH₂-CH₃ TSAO-e³T

Figure 1. Chemical formulas of TSAO derivatives.

nucleoside and non-nucleoside inhibitors,¹² and for this reason, the search for new drugs and alternative targets is amply justified.

[2',5'-Bis-*O*-(*tert*-butyldimethylsilyl)- β -D-ribofuranosyl]-3'-spiro-5''-(4''-amino-1'',2''-oxathiole-2'',2''-dioxide)thymine (TSAO-T, Figure 1) is the prototype of a unique class of nucleoside analogues that have been identified as highly specific noncompetitive inhibitors of the RNA-dependent DNA polymerase function of HIV-1 RT.^{13,14} Resistance of HIV-1 RT against the TSAO class of inhibitors is principally determined by the Glu-138 \rightarrow Lys mutation.¹⁵ This glutamic acid residue is present in the β 7– β 8 loop⁵ of the p51 subunit and has long been thought to interact specifically with the 4''-amino group on the 3'-spiro-substituted ribose moiety of the TSAO nucleosides,¹⁶ although the precise binding mode has not yet been elucidated. Both TSAO-T and its N3-ethyl derivative (TSAO-e³T) have recently been shown to enhance the urea¹⁷ or acetonitrile-mediated^{17,18} destabilization of both the p66–p51 heterodimer and the p66–p66 homodimer in a concentration-dependent manner, leading to a loss in their ability to bind DNA.¹⁸ On

* To whom correspondence should be addressed: Departamento de Farmacología, Universidad de Alcalá, E-28871 Alcalá de Henares, Madrid, Spain. Telephone: +34-918 854 514. Fax: +34-918 854 591. E-mail: federico.gago@uah.es.

[†] Universidad de Alcalá.

[‡] CSIC.

[§] Katholieke Universiteit Leuven.

the other hand, TSAO-e³T was unable to destabilize the subunit interactions of the E138K mutant enzyme.¹⁷

A preliminary molecular model of the RT–TSAO complex placed TSAO-T near the interface between the p66 (A) and p51 (B) subunits with most of the molecule located inside the standard NNRTI binding pocket in p66.¹⁹ For the purpose of validation, we designed modifications on both the inhibitor and the enzyme. On one hand, it was inferred from the model that removal of O4 of the pyrimidine ring in TSAO-T would lead to an increase in binding affinity. The rationale was that the negative electrostatic potential generated in this region of the inhibitor was detrimental for binding as this oxygen was close to the main chain carbonyl group of His-A235. On the other hand, the model suggested that mutation of Arg-A172 to Ala would decrease the affinity for TSAO compounds but would not affect the binding of other NNRTIs. The rationale in this case was that the negative electrostatic potential generated by the solvent-exposed sulfone group of TSAO²⁰ could give rise to a favorable interaction energy with the positively charged side chain of Arg-A172 (or Lys-A172 in other HIV-1 strains). We now report that in both these instances the molecular model was not corroborated by the experimental results. This led us to explore alternative binding modes and to study the energetics of dimerization and the rationale for the effects of TSAO-T on RT dimer stabilization. The docking strategy consisted of extending the putative binding site further away from the standard NNRTI binding pocket and using all the reported X-ray crystal structures of the enzyme, both complexed with other inhibitors and in the apo form, as input for an automated docking program. One of the binding modes that was obtained was consistent with available structure–activity and mutagenesis data,^{21–24} and provided strong evidence that TSAO analogues may indeed bind at the interface between the two subunits but in a manner that does not make use of the NNRTI binding pocket. In fact, a structure-based chemical modification introduced in the lead compound, TSAO-T, led to a slight improvement in activity, in accord with our expectations from the new molecular model.

Results

(a) Study of the RT Dimer Interface. Upon formation of the heterodimer from p66 and p51 monomers, a large surface of RT becomes inaccessible to water. Our estimates range from ~4300 Å² (PDB entry 3hvt)⁵ to ~5300 Å² (PDB entry 1rtj)⁴ of buried protein surface area depending on the source of the structure, of which ~2800 and ~3300 Å², respectively, correspond to non-polar atoms. The calculated contribution of the ensuing hydrophobic effect to dimer stabilization, the entropy of immobilization notwithstanding, comes to about 56–66 kcal mol⁻¹. That other factors are at play is highlighted by the fact that the experimental free energy of dissociation has been estimated to be ~10 kcal mol⁻¹.^{17,25} Dissecting the contributions of individual residues to the buried surface area upon binding reveals important intersubunit contacts (Figure 1 of the Supporting Information). Particularly noticeable (>100 Å²) are Trp-A88, Trp-A406, Ala-A408, and Trp-A410 in the p66

subunit and Pro-B52, Asn-B136, Asn-B137, Glu-B138, Thr-B286, and Trp-B401 in the p51 subunit. Of direct interest to us is the segment from Ile-B135 to Pro-B140, which is part of the β7–β8 loop and includes Glu-B138. The tip of this loop is very close to the NNRTI binding site and fits into the floor of the polymerase cleft of the p66 subunit so that it is partly buried upon dimerization.

Since it has been demonstrated that buried surface area alone may not correlate well with the functional importance of a given interface residue,²⁶ we calculated the van der Waals and electrostatic contributions to the binding enthalpy (Figure 2 of the Supporting Information) both for the wild-type enzyme and for the E138K mutant that arises under selective pressure by TSAO derivatives. To test the effect of replacing Glu-B138 with a lysine, the side chains of the mutated form of the enzyme were allowed to reorientate in the presence of water molecules. Interestingly, the overall p66–p51 interaction energy was found to be very similar in both enzymes, in agreement with the experimental finding that only 0.35 kcal mol⁻¹ in free energy of dimerization is lost in the E138K mutant with respect to the wild-type RT.¹⁷ There are very few significant differences in the van der Waals components, whereas compensations are detected in the electrostatic contributions: most importantly, the favorable interaction of Glu-B138 with Lys-A101 and Lys-A103 that is lost in the E138K mutant relative to wild-type RT is replaced, even in the presence of water molecules, with both an improved interaction between the ε-amino group of Lys-B138 and the carbonyl group of Gly-A99 and a more favorable interaction between Lys-B49 and Glu-A169. Besides, it must be noted that part of the stabilizing energy for dimerization provided by amino acid residue B138 arises from the interaction between its backbone carbonyl group and the backbone NH of Gln-A182. As a result of these changes, no decrease in the level of dimer stabilization would be expected upon mutation, in apparent good agreement with the experimental findings.¹⁷

(b) Conformational Studies on TSAO-m³T. The high degree of functionalization on the sugar ring precludes large conformational freedom in TSAO-m³T, but the ligand is still endowed with some flexibility so that it is able to place the different substituents and functional groups in slightly different locations relative to one another. This limited flexibility arises from (i) rotation of the thymine base of TSAO-m³T about the glycosyl C1'–N bond, which gives rise to either a syn or an anti orientation relative to the ribose, (ii) repuckering of the sugar ring, and (iii) rotation of the *tert*-butyldimethylsilyl (TBDMS) substituents attached to the oxygens at positions 2' and 5' of the ribofuranose. Representatives of both syn and anti conformational families were found among the low-potential energy structures of TSAO-m³T, and the puckering modes most frequently observed for the sugar ring were O4'-*endo*, C2'-*endo*-C3'-*exo*, and C3'-*endo*, in broad agreement with results from NMR experiments and MD simulations in different solvents.²⁷ Although the syn conformer would be expected to be preferentially stabilized in vacuo by the favorable enthalpy provided by the intramolecular hydrogen bond between O2 of thymine and the amino group on the spiro moiety, this contribution is surely

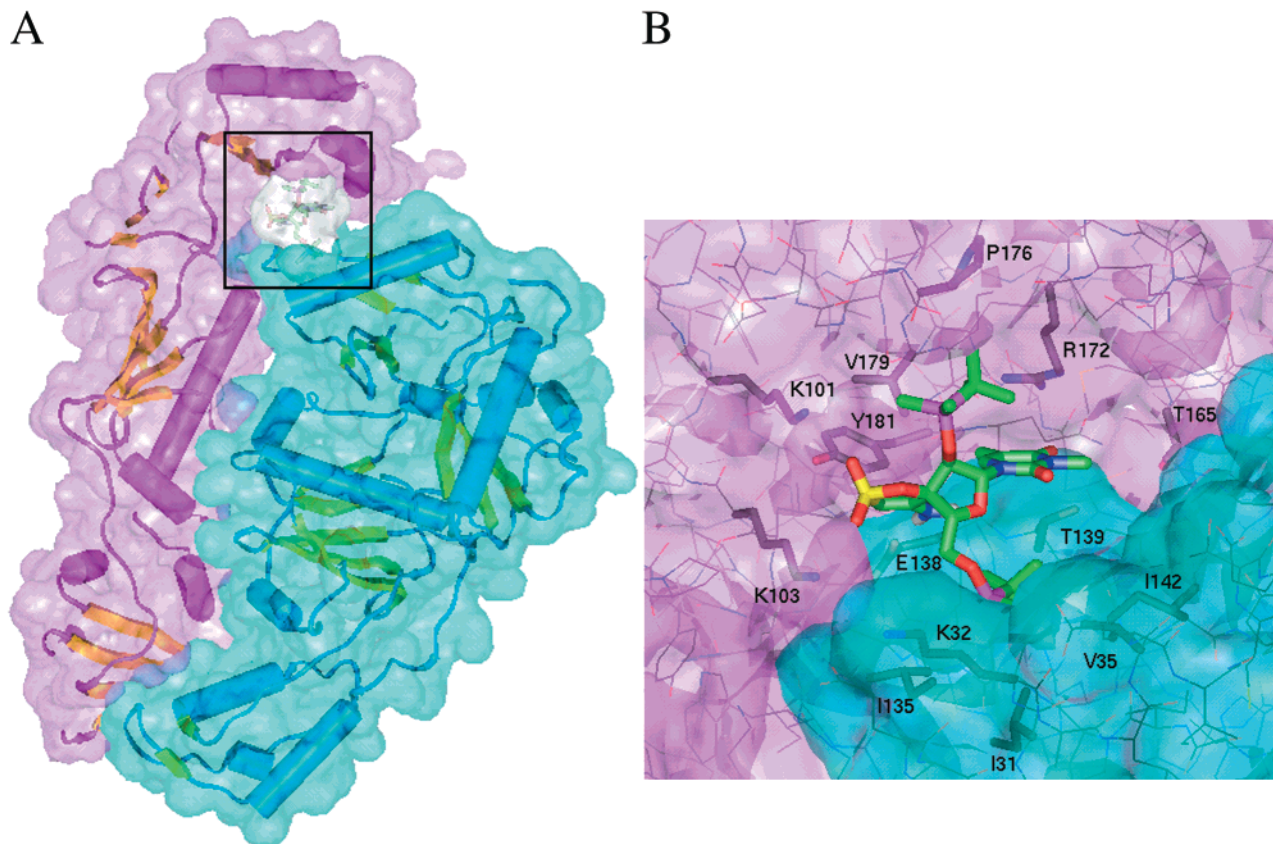


Figure 2. Proposed binding site for TSAO- m^3T at the p66–p51 interface of HIV-1 RT. (A) Schematic representation of the C_α trace of HIV-1 RT (α -helices are shown as barrels and β -strands as flat ribbons), with p66 and p51 residues enveloped by a solvent-accessible surface colored in pink and blue, respectively. A similar gray surface surrounds the inhibitor. (B) Enlarged view of the framed area shown in panel A. Protein residues relevant to the discussion have been labeled, and their side chains are shown as sticks.

counterbalanced by a less favorable electrostatic solvation energy, which may account for the syn–anti equilibrium mixture that is actually detected in solution.²⁷ In addition, rotation about the exocyclic C4′–C5′ bond allows O5′ to assume different positions relative to the furanose, which are described by torsion angle γ (O5′–C5′–C4′–C3′),²⁸ including one in which this oxygen hydrogen bonds the spiro amino group, as found in the reported X-ray crystal structure of TSAO- m^3T .¹⁷ These hydrogen bonds are therefore thought to have a strong influence on the puckering mode of the sugar.²⁷

(c) Docking Studies. For the NNRTIs used as controls in the docking experiments, the X-ray solution was found as the best hit in all cases [root-mean-square deviation (rmsd) < 1.0 Å] provided the protein used as the target was that found in the crystallographic structure of the corresponding RT–NNRTI complex. For alternative protein targets, the performance depended on the extent of conformational change induced by the ligand upon binding. Thus, nevirapine could be correctly docked into most of the other RT targets containing a preformed NNRTI binding pocket, but U90152 strictly needed its own enlarged binding site.⁵⁵ As for TSAO- m^3T , a wide variety of binding modes was found by the automated docking method in the region delimited for exploration, but most of them could be disregarded for being incompatible with the rather stringent structure–activity relationships (SARs) known for this class of inhibitors.^{19–24} Notable differences in docking orientations and binding modes were found depending on the

source of the RT structure (data not shown). One of the highest scores for TSAO- m^3T compatible with the SARs was obtained when the apoenzyme was used as the target protein. In the orientation that was found, TSAO- m^3T does *not* make use of the NNRTI binding pocket. Instead, it binds at the interface between the two subunits (Figure 2) in such a way that the strong dipole moment of the spiro group ($\mu = 8.4$ D)²⁰ of TSAO- m^3T is properly aligned in the field created by the positive electrostatic region emanating from Lys-A101 and Lys-A103 in the p66 subunit and the negatively charged Glu-B138 in the p51 subunit. An additional polar interaction is formed between O4 of the thymine ring and the hydroxyl group of Thr-B139 in the p51 subunit. The remaining stabilizing interactions are hydrophobic and exploit two cavities present at the enzyme interface that provide binding pockets for the 2′- and 5′-TBDMS substituents of TSAO derivatives. In the p51 subunit, the side chains of Ile-B31 and Val-B35 and the hydrocarbon side chains of Lys-B32 and Ser-B134 provide a large hydrophobic surface that accommodates the indispensable 5′-TBDMS substituent.²¹ In the p66 subunit, the hydrophobic pocket is made up mainly by Pro-A176 and Val-A179, both of which interact with the 2′-TBDMS group. The total amount of protein surface area buried upon complexation with TSAO- m^3T amounts to ~ 460 Å² (Table 1), of which ~ 300 Å² corresponds to apolar surface area ($\sim 50\%$ from each subunit), which sets an upper limit of ~ 6 kcal mol⁻¹ to the entropic contribution to the free energy of binding.

Table 1. Solvent-Accessible Surface Area (Å²) Buried upon Binding of TSAO-m³T to Wild-Type RT

	p66 Subunit											
	K101	K103	T165	R172	K173	P176	I178	V179	I180	Y181	Q182	P321
polar	14.0	0.4	0.0	36.2	21.7	15.5	7.6	0.0	3.4	5.9	0.7	0.0
apolar	10.9	0.0	9.4	21.4	14.0	17.7	0.0	54.4	0.0	19.6	0.0	0.3
total	24.9	0.4	9.4	57.6	35.7	33.2	7.6	54.4	3.4	25.5	0.7	0.3
	p51 Subunit											
	E28	I31	K32	V35	S134	I135	E138	T139	I142			
polar	8.6	0.0	0.0	0.0	0.0	1.6	31.9	7.3	0.0			
apolar	5.9	14.7	17.0	29.3	5.7	14.0	6.6	52.8	14.6			
total	14.5	14.7	17.0	29.3	5.7	15.6	38.5	60.1	14.6			

Table 2. RT Inhibitory Activity of TSAO-T Analogues on Wild-Type and Mutant Enzymes

	IC ₅₀ (μg/mL) ^a		
	wild type	E138K	R172A
TSAO-T (1) ^b	3.6 ± 0.2	>500	0.37 ± 0.0
TSAO-m ³ T ^b	2.8 ± 0.18	>500	0.42 ± 0.01
UC-781	0.008 ± 0.0008	0.076 ± 0.014	0.007 ± 0.0001
delavirdine	0.30 ± 0.07	1.96 ± 0.30	0.18 ± 0.01
efavirenz	0.007 ± 0.004	0.007 ± 0.0001	0.003 ± 0.0008
ddGTP ^b	0.42 ± 0.04	0.43 ± 0.06	0.54 ± 0.06

^a Concentration required to inhibit the RT reaction by 50%. ^b In micromolar.

(d) In Vitro Inhibition of Wild-Type and Mutant RT Enzymes by TSAO and Other NNRTIs. The prototype TSAO-T and TSAO-m³T were equipotent in their inhibition of HIV-1 RT (Table 2), as described previously,²⁹ and the E138K mutation resulted in the already reported dramatic loss of inhibitory activity.^{15,16} The sensitivity of the R172A mutant RT, on the other hand, was virtually unchanged for all the HIV-1-specific NNRTIs assayed except for the TSAO derivatives which, interestingly, inhibited the mutant enzyme to a markedly larger extent (7–10-fold) than the wild-type enzyme (Table 2).

(e) Molecular Dynamics Simulations and Analyses of Wild-Type and R172A Mutant Enzymes and Their Complexes with TSAO-m³T. To validate and test the stability of the proposed binding mode, a MD trajectory was simulated in which positional restraints on both the ligand and the protein were progressively reduced and finally removed. For the whole length of the simulation with the wild-type enzyme, TSAO-m³T remained docked in the binding site conserving the same initial conformation (rmsd < 0.5 Å for all non-H atoms and excluding equivalent methyl groups) except for a minor adjustment of the 5'-TBDMS substituent after 860 ps brought about by a change in the C5'-O5'-Si-C torsional angle from the original value of ~120° to ~60°. This same rotation was observed in the complex with the R172A mutant RT after 1260 ps.

The evolution of the rmsd of the atoms of the protein backbone reflected the strength and duration of the positional restraints that were used, and were similar for the free proteins and their complexes with TSAO-m³T (Figure 3 of the Supporting Information). Thus, for the first 1260 ps this rmsd was ~0.7 Å with respect to the initial energy-minimized structure. When the β7–β8 loop and the β strands containing the catalytic Asp residues were freed, the rmsd increased to ~0.8 Å, and remained at ~1.3 Å for the rest of the unrestrained MD

simulation. This final rmsd was slightly higher (~1.6 Å) in the simulation of the complex with the R172A mutant.

The histograms in Figure 3 allow for a rapid inspection of the van der Waals and electrostatic contributions of individual residues to the binding energy. The major van der Waals interactions are nicely coincident with the extents of buried surface area (Table 1). The most important electrostatic contribution turns out to be precisely with Glu-B138, followed by Lys-A101 and Lys-A103, and by Thr-B139; remarkably, this interaction is unfavorable for Arg-A172 and almost negligible for Ala-A172 in the mutant enzyme. The distances separating the N ζ atoms of Lys-A101 and Lys-A103 and the sulfone oxygens (4.4 ± 0.5 and 3.3 ± 0.8 Å, and 4.6 ± 0.6 and 6.5 ± 0.6 Å, respectively) are slightly too long during most of the simulation to consider these interactions as hydrogen bonds. On the other hand, strong hydrogen bonds can be inferred from the proper orientations and short distances (2.7 ± 0.2 and 2.8 ± 0.1 Å, respectively) between the spiro amino group and the carboxylate of Glu-B138 and between the O4 of the thymine ring and the hydroxyl group of Thr-B139 in the p51 subunit.

The dipolar nature of TSAO derivatives is clearly visualized in Figure 4; the molecular electrostatic potential (MEP) calculated for TSAO-m³T shows the most negative region (pink) surrounding the spiro oxathioldioxide group, the O2' and O5' sugar atoms, and the thymine O2 atom, whereas the most positive region (blue) appears in the vicinity of the spiro amino group. A small blob of negative MEP can also be observed emanating from the thymine O4 atom between the two pyrimidine methyl groups. We believe it is this MEP distribution, together with the hydrophobic effect, that favors positioning of the drug in the proposed binding site. With regard to the enzyme, when the MEPs of wild-type and E138K mutant enzymes were compared, a very significant difference was found spreading over a region surrounding the carboxyl group of Glu-B138 (Figure 4 of the Supporting Information). This finding, together with the fact that a consistently favorable and large electrostatic interaction energy was calculated between Glu-B138 and TSAO-m³T during the whole length of the MD simulations (Figure 3), may account for the pronounced loss of binding affinity of TSAO derivatives on the E138K mutant enzyme (Table 2).^{15,17} Further support for the importance of this interaction was recently obtained when the inhibitory activity of both TSAO-T and TSAO-m³T against E138A mutant HIV-1 RT was shown to be reduced 30–100-fold relative to the wild-type enzyme.³⁰ In fact, residue 138 in HIV-2 RT is an

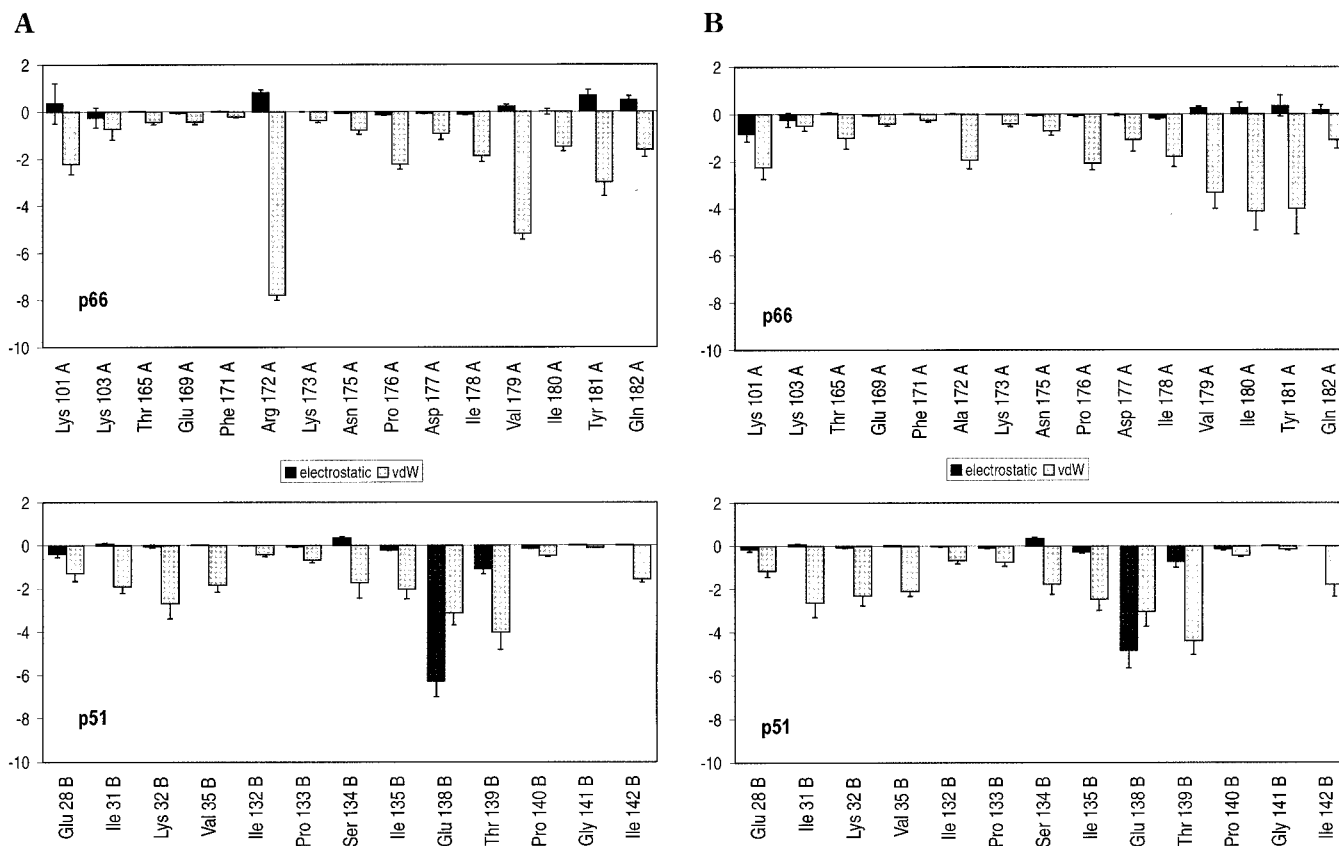


Figure 3. Residue-based van der Waals and electrostatic contributions to the binding of TSAO-m³T to (A) wild-type and (B) R172A mutant HIV-1 reverse transcriptase.

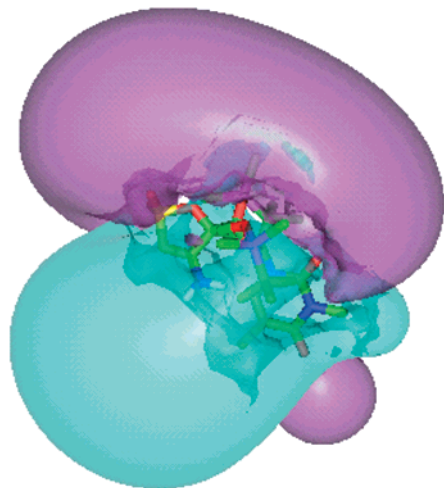


Figure 4. Molecular electrostatic potential of TSAO-m³T represented as two semitransparent contours surrounding a stick representation of the molecule (nonpolar hydrogens have been omitted for clarity). Negative (-0.1 to -3.2 kcal mol⁻¹) and positive regions (0.1 – 10.3 kcal mol⁻¹) are colored in pink and blue, respectively.

alanine, and TSAO derivatives are highly specific against HIV-1.

With respect to the effect of the R172A mutation on TSAO-m³T binding, the MD simulation of this complex showed a similar drug binding orientation and overall interaction energies as described for the wild-type enzyme (Figure 3). Significant differences were observed for only a few residues, as probably expected for a point mutation. Most noticeable was the loss of van der Waals

interactions upon replacement of Arg with Ala at position 172, although this loss was partially compensated with a better interaction of TSAO-m³T with the neighboring Ile-A180. On the other hand, the electrostatic term involving the Ala-A172 residue was seen to improve even though the overall electrostatic interaction energy between TSAO-m³T and the protein, calculated with the continuum method, was similar for both the wild-type and the R172A mutant enzymes (-5.8 ± 1.4 vs -5.7 ± 1.4 kcal mol⁻¹, respectively). A large difference was found, however, when the electrostatic contribution to the desolvation energy of this amino acid residue was calculated (5.13 ± 0.75 kcal mol⁻¹ for Arg vs 0.25 ± 0.12 kcal mol⁻¹ for Ala).

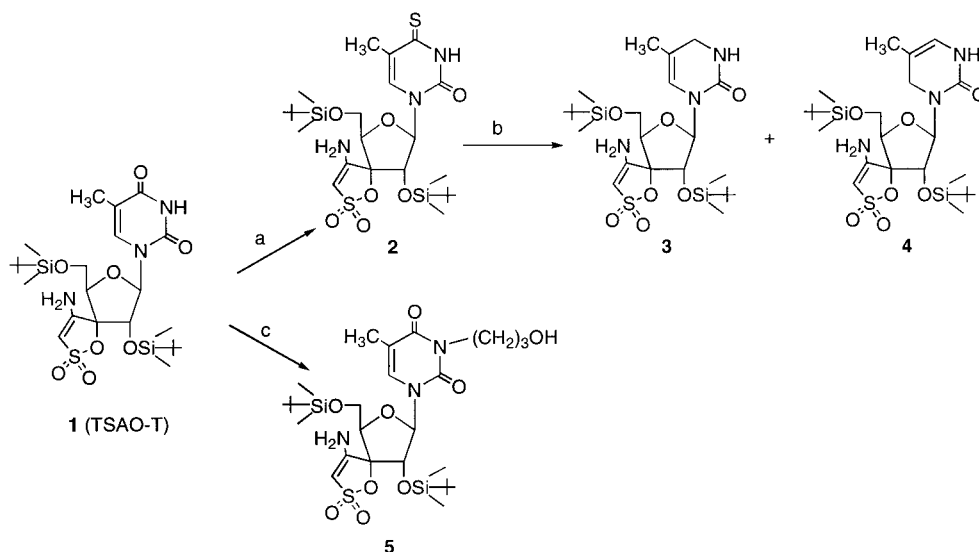
(f) Suggested LUDI Modification of TSAO-T. According to the docking model, additional interactions at or near the p51–p66 interface could result in compounds with improved binding affinity over the prototype TSAO-T. Different fragments were suggested by LUDI for attachment at the N-3 position of the thymine ring (Table 3). Target functional groups on the enzyme were the carbonyl oxygen of Pro-A140, the terminal amino group of Lys-B49, the carboxylate group of Glu-A169, and the apolar side chain of Ile-B142. For ease of synthesis, the (CH₂)₃-OH substituent was chosen as the resulting molecule could be readily prepared in one step following our previously described method for the selective N-3 alkylation of TSAO derivatives.²⁹

(g) Synthesis and Antiviral Activity of Novel TSAO Compounds. Removal of the 4-oxo group from the thymine ring of TSAO-T was achieved in two steps (Scheme 1) by initial thiation of TSAO-T (1) followed by reductive desulfurization of the 4-thiocarbonyl group

Table 3. Substituent Fragments Suggested by the LUDI Program for Attachment to the N3 Position of TSAO-T

id	Fragment	# hb ^a	Target ^b	id	Fragment	# hb ^a	Target ^b
I		1	CO Gly-B141	V		1	CO Pro-A140
II		1	NH3 Lys-B49	VI		1	COO ⁻ Glu-A169
III		1	CO Pro-A140	VII		0	Ile-B142
IV		0	Ile-B142	VIII		1	CO Pro-B140

^a Number of hydrogen bonds. ^b Target functional group on the receptor.

Scheme 1^a

^a Reaction conditions: (a) Lawesson's reagent, toluene, Δ ; (b) $\text{NiCl}_2 \cdot 6\text{H}_2\text{O}$, MeOH/THF, NaBH_4 ; (c) $\text{Br}(\text{CH}_2)_3\text{OH}$, K_2CO_3 , acetone.

using "nickel boride" as the reducing agent.³¹ Use of this reagent allows reduction under smooth conditions, whereas the widely employed Raney nickel gives complex mixtures of products, as described for the conversion of 4-thiothymine nucleoside derivatives into the corresponding 2-pyrimidone derivatives.³² Thus, treatment of **1** with Lawesson's reagent under standard conditions³³ gave the 4-thioderivative **2** in 60% yield. When **2** was reacted with nickel boride, generated in situ by the action of sodium borohydride on nickel(II) chloride, the 3,4-dihydro-5-methyl-2-pyrimidone derivative **3** and the corresponding 3,6-dihydro-5-methyl-2-pyrimidone derivative **4**, produced by migration of the 2-pyrimidone double bond, were isolated in 25 and 20% yield, respectively. Scarce examples of double bond migration in reductive desulfurization reactions using nickel boride have been previously described in the literature.³⁴ The structures of compounds **3** and **4** were unambiguously determined by extensive and full spectroscopic analysis (¹H NMR, ¹³C NMR, ¹H-¹H COSY,

HSQC, HMBC, and NOE experiments). The N-3-substituted derivative **5** suggested by LUDI was synthesized in 78% yield (Scheme 1) by treating **1** with 3 equiv of 3-bromopropanol in dry acetone and in the presence of potassium carbonate (K_2CO_3).

When compounds **2-4** were tested against HIV replication, a ~3-fold decrease in inhibitory potency with respect to the prototype TSAO-T was found (Table 4). This result is fully compatible with the loss of the proposed hydrogen bond between O4 and the hydroxyl group of Thr-B139 in the model presented here. On the other hand, attachment of a $(\text{CH}_2)_3\text{-OH}$ substituent to the thymine N3 atom of TSAO-T to yield compound **5** resulted in a 2-fold better inhibitor, consistent with the prediction that an additional hydrogen bond could be formed with the carbonyl group of Pro-B140.

Discussion

Our previous working model^{19,22,23} placed the essential 5'-TBDMS substituent of TSAO-T in the cavity formed

Table 4. Inhibitory Activity of TSAO Derivatives against HIV-1 and HIV-2 in CEM and MT-4 Cell Cultures

compd	EC ₅₀ (μM) ^a			
	MT-4		CEM	
	HIV-1	HIV-2	HIV-1	HIV-2
2	0.17 ± 0.05	>10	0.17 ± 0.05	>2
3	0.20 ± 0.03	>10	0.10 ± 0.0	>2
4	0.23 ± 0.06	>10	0.12 ± 0.0	>10
5	0.03 ± 0.003	>2	0.01 ± 0.006	>2
TSAO-T	0.06 ± 0.03	>20	0.06 ± 0.01	>20
TSAO-m ³ T	0.05 ± 0.01	>200	0.06 ± 0.09	>200

^a The 50% effective concentration, or the concentration required to protect 50% of the virus-infected cells against destruction by the virus.

by Tyr-A181, Tyr-A188, and Trp-A229 and placed the thymine ring close to Tyr-A318, with substituents on the N3 position pointing toward a channel connecting the binding pocket with the solvent. In this orientation, the spiro amino group was able to form a good hydrogen bond with the carboxyl group of Glu-A138 in the p51 subunit, and this important interaction was thought to lie at the origin of the E138K mutation detected under the selective pressure of TSAO derivatives.¹⁵ Despite the relative success of this model in accounting for many experimental findings,¹⁹ some data argued against it. One piece of contradictory data came from early experiments showing that TSAO-e³T could not protect either free RT or the RT–template-primer–deoxynucleoside triphosphate ternary complex from irreversible inactivation by the photolabel 9-azidonevirapine, suggesting that TSAO-e³T and typical NNRTI such as nevirapine might bind to distinct sites on RT.³⁵ Nor was it possible for several TSAO derivatives to soak out a weak binding NNRTI such as HEPT from pregrown crystals to cocrystallize with RT.³⁶ More recently, biochemical experiments showed that TSAO binding to RT is accompanied by dimer destabilization, which would be at odds with a binding model in which the bulk of TSAO-T is lodged in subunit p66 attracting toward it Glu-B138 from the p51 subunit, intuitively stabilizing the dimer. Undoubtedly, our early model was strongly biased by attempts to make use of the NNRTI binding pocket, as seen in the structures of many complexes determined by X-ray crystallography and consistently reproduced in our hands by the docking programs when applied to many other NNRTIs. However, no solution was afforded by any of the programs used when this pocket was targeted as the binding site for the bulky TSAO-T as a whole, and only partial fragment-based solutions were obtained.^{22,23}

The final evidence that convinced us that our previous model could not be correct is presented here. Removal of the oxygen atom from position 4 of the thymine ring in **1** to yield **3** and **4** resulted in a loss of activity (Table 4) rather than in an increment, as would have been expected on the basis of the former model. Moreover, replacement of the arginine at position 172 with an alanine in RT led to an unanticipated improvement in the inhibitory activity of TSAO analogues (Table 2).

In light of all these experimental data, we tried to find an alternative binding mode. The protein region used in the docking experiments was expanded, and all the available structures of RT either alone or in complex with inhibitors or DNA were used in the search. As a

result, a new binding mode is now presented that is in agreement not only with previous evidence but also with the new experimental data reported herein. In the updated model, TSAO-m³T straddles between subunits binding at the p66–p51 interface but it does not make use of the NNRTI binding pocket. The importance of the thymine O4 is now highlighted, as it is proposed to establish a good hydrogen bond with the side chain of Thr-B139 so that its removal is detrimental to activity. It will be interesting to explore by site-directed mutagenesis the importance of this residue for TSAO binding. The effect of replacing Arg-A172 with Ala is likewise accounted for; in the wild-type enzyme, a large van der Waals contribution to TSAO-m³T binding is calculated for this residue, mainly due to the stacking of the guanidinium group (held in place by two hydrogen bonds to the carbonyl oxygen of Ile-A180 and the OE1 atom of Gln-A182) over the pyrimidine ring of TSAO, but the electrostatic term is shown to be slightly repulsive (Figure 3). This unfavorable binding energy component was shown to be further aggravated by the penalty incurred on desolvation of such a positively charged group in the absence of a compensating negative charge. Avoidance of this desolvation penalty upon replacement of this residue with an alanine, together with the improved electrostatic interaction (Figure 3), may account for the enhanced TSAO inhibition observed for the R172A mutant enzyme (Table 2).

If the model presented here is correct, all of the active compounds in the TSAO series are highly preorganized for binding to this site due to the high degree of functionalization of the ribose, which surely implies a rather small loss of conformational entropy upon binding. On the other hand, a large favorable entropy change can be foreseen from the desolvation of all the nonpolar groups upon complex formation.

The proposed binding mode accounts for the structure–activity data on the extensive series of more than 400 TSAO analogues synthesized to date.¹⁹ In particular, the molecular model presented here rationalizes the crucial role played by the essential TBDMS substituent on the 5' side of TSAO, and at the same time explains why a larger *tert*-hexyldimethylsilyl substituent is also accepted at this position with only a marginal loss of activity.²¹ The numerous contacts that have been identified may account for the very stringent requirement for this group at this position which cannot accommodate any structural variation without a loss of affinity. The model also adequately explains why more chemical variation is possible on the 2' substituent,²¹ and why the N3 position on the pyrimidine ring can accept such a large chemical diversity, ranging from a methyl group to larger groups¹⁹ and very long chains, as in the reported active TSAO–AZT and TSAO–d4T heterodimers.^{20,24} In light of the model presented here, these N3 substituents would be found running parallel to the subunit interface and mostly exposed to the solvent, thus making an almost negligible or at worst a slightly deleterious contribution to binding. Solvent exposure is probably one of the reasons why the structure-based modification introduced in TSAO-T to yield **5** led to only a relatively modest improvement in activity. The putative extra hydrogen bond with the protein backbone may be partially offset by the inherent flexibility of the

methylene linker and by competition with surrounding water molecules. Synthetic efforts are underway to further explore new anchoring points along the interface cleft.

The model presented here provides a detailed molecular-level picture in line with previous suggestions about the $\beta 7$ – $\beta 8$ loop being the binding site for TSAO derivatives^{15a,18} and has many features in common with an independent model recently outlined for TSAO- e^{3T} binding to HIV-1 RT based on the $C2'$ -endo conformation of TSAO- m^{3T} found in the X-ray crystal structure.¹⁷ In this latter work, the dimerization interface in the $\beta 7$ – $\beta 8$ loop region was suggested as the target site for TSAO analogues and there are strong similarities with our model regarding the protein residues that are thought to contact the inhibitor. Nevertheless, no details of the docking procedure or the nature and magnitude of the interactions with different protein residues were provided. We now show that the docked conformation of TSAO- m^{3T} differs from that found in the crystal structure of the isolated drug molecule, and that binding to this novel site appears to be driven mostly by well-defined electrostatic steering and hydrophobic interactions with a rather large set of amino acids from both p66 and p51 subunits.

With regard to the mechanism by which TSAO derivatives exert their inhibitory action, it has been suggested that the presence of the drug at the interface between the two subunits may perturb the dynamics of subunit association and/or prevent the conformational changes necessary for loading the p66 subunit onto the template-primer complex. In fact, it has been demonstrated that the heterodimeric enzyme shows a reduced DNA binding ability in the presence of a 5-fold molar excess TSAO-T⁷ and also that TSAO- e^{3T} can induce the dissociation of RT into inactive monomers under certain conditions.³⁷ By studying the residues that are involved in dimer formation, we have identified the $\beta 7$ – $\beta 8$ loop in the p51 subunit as an important component of the dimerization interface (Figures 2 and 3 of the Supporting Information). Interestingly, Glu-B138, the residue that is found mutated to Lys in TSAO-resistant viruses, is located in this loop, and our results with the E138K mutant enzyme are consistent with the experimental results which show that this substitution drastically reduces the affinity of TSAO derivatives¹⁵ and at the same time does not lead to gross changes in dimerization binding energy.¹⁷ Nevertheless, dissociation of the subunits does not appear to take place in the absence of denaturant, and the concentrations of TSAO- m^{3T} that are necessary to produce this effect are higher than those needed to display inhibitory activity.

How do TSAO derivatives then exert their inhibitory action? For RT inhibition by classical NNRTIs, it has been suggested that the most dramatic change in the protein relative to the apoenzyme is the concerted movement of strands $\beta 6$, $\beta 9$, and $\beta 10$, which contain the functional aspartic acid residues (Asp-A110, Asp-A185, and Asp-A186) that comprise part of the polymerase active site.³⁸ By comparing our simulations of wild-type HIV-1 RT in the presence and in the absence of bound TSAO- m^{3T} , we noticed a similar disorganization of the catalytic aspartates (Figure 5), although it is achieved through a different mechanism. The $\beta 7$ – $\beta 8$ loop remains

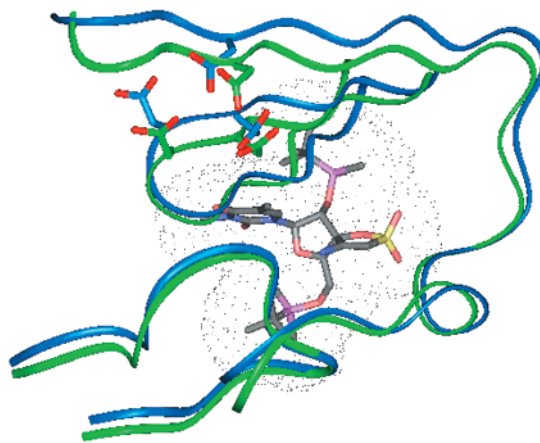


Figure 5. Comparison of the active site region containing the catalytic aspartate residues in the reduced model structures of free (blue) and TSAO-bound HIV-1 RT (green). Each snapshot is representative of the last 2 ns of each MD simulation and was taken 400 ps before the end of the trajectory. Only the C_{α} traces used in the superposition are shown, together with the side chains of the catalytic aspartate residues and the non-H atoms of TSAO- m^{3T} (gray carbon atoms and dotted surface).

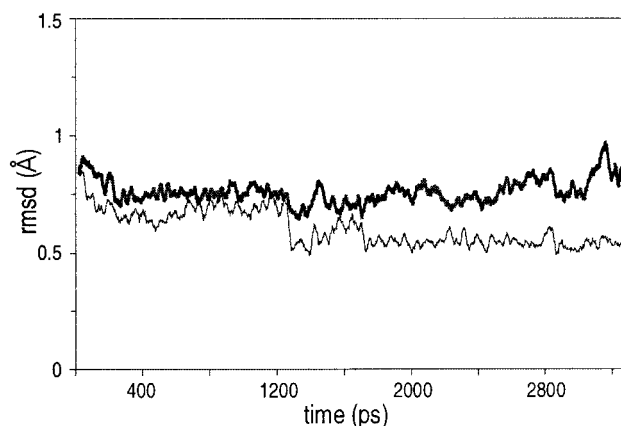


Figure 6. Time evolution of the root-mean-square deviation (rmsd) of C_{α} atoms in the $\beta 6$, $\beta 9$, and $\beta 10$ strands from equivalent atoms in the catalytically active RT structure as reported in ref 3b: free (thin line) and TSAO-bound HIV-1 RT (thick line).

essentially unchanged, but the “pulling” interaction of TSAO- m^{3T} with Lys-A101 and Lys-A103 gives rise to changes in both the $\beta 5$ and $\beta 6$ strands. On the other hand, the pushing interaction with Val-A179 and Pro-A176 determines a displacement of the $\beta 9$ and $\beta 10$ strands and the α -helix immediately preceding $\beta 9$. When the trace of C_{α} atoms in these β -strands of both free and TSAO-bound RT are compared to that of equivalent atoms in the catalytically active conformation of RT bound to DNA,^{3b} the rmsd is shown to decrease only during the simulation of the apoenzyme (Figure 6). Although these results should be viewed with caution, given the limitations of the reduced models that were used, it is tempting to speculate that the presence of TSAO at the subunit interface may preclude adoption by the enzyme of the catalytically active conformation. In this dynamic context, the presence of additional residues not directly in contact with the TSAO molecule could be important in the inhibition mechanism as cross resistance to TSAO derivatives has been seen in mutants selected by other NNRTIs, such as those involving

positions 106, 181, and 188, which are within the standard NNRTI binding site.³⁹

Conclusions

The binding mode of the unique TSAO series of RT inhibitors has proved to be elusive for some time as repeated attempts to cocrystallize TSAO-T and other TSAO derivatives with HIV-1 RT have not yet met with success.³⁶ Computational docking studies have found it necessary to expand the putative binding region beyond the NNRTI binding pocket and have led us to propose a binding mode for TSAO-m³T that is novel and quite distinct from that of "classical" NNRTIs. The new molecular model is in agreement with the biochemical evidence and with known structure-activity and mutagenesis data for this class of inhibitors, including a R172A mutant that had not been described previously. The feasibility of the proposed binding mode was assessed by analyzing the results of nanosecond MD simulations for the complexes of TSAO-m³T with reduced models of the wild-type and R172A mutant RT enzymes in the presence of water molecules. The cost of desolvating the side chain of this arginine residue was shown to be unfavorable for complex formation, and this is suggested to be the main reason accounting for the unanticipated improved binding of TSAO-m³T to the R172A mutant enzyme.

TSAO-m³T is shown to be a relatively hydrophobic ligand²⁰ with severely reduced flexibility whose conformation is preshaped to the geometry of its putative binding site, which is proposed to be at the interface between the p66 and p51 subunits of HIV-1 RT. A structure-based modification introduced on this lead compound led to a new derivative (5) that exhibited a 2–6-fold improvement in antiviral potency. In addition to suggesting new site-directed mutations and providing fertile ground for further modifications in this series, the current model points to a well-defined part of the dimerization interface as a novel target for inhibitor design. To our knowledge, TSAO-T is the first example of a small nonpeptidic molecule that can interfere with the dimerization process and can thus be used as a lead compound for the design of an entirely new family of RT inhibitors that would act independently of both the active site and the NNRTI binding pocket.

Experimental Section

A. Theoretical Methods. a. Solvent-Accessible Surface Calculations. The reduction in protein solvent-accessible surface area (SA) brought about by dimerization was calculated as the difference between the total SA of the dimer and the summed SA of the two isolated subunits⁵ using the program NACCESS⁴⁰ and a water probe with a radius of 1.4 Å.⁴¹ The protein SA buried upon ligand binding was calculated as the difference in SA of the protein in the absence and in the presence of TSAO-m³T. The magnitude of the hydrophobic effect involved was calculated making use of the conversion factor of 20 cal/Å² obtained from a linear correlation between the SA of hydrophobic side chains and their free energy of transfer from a polar to a nonpolar solvent.⁴²

b. Reduced Models of Wild-Type and Mutant RT Enzymes. For the docking experiments and subsequent computational work, we focused on a reduced model of RT comprising the NNRTI binding site and all those residues within 30 Å of Glu-B138. The number of fragments was kept to a minimum by including some additional connecting residues, and the resulting peptide chains were capped with

suitable acetyl and *N*-methyl groups in place of the preceding and following amino acids, respectively.⁴³ All in all, 322 protein residues were considered (A4–A11, A85–A122, A147–A247, A260–A276, A305–A329, A338–A354, A372–A389, B14–B62, and B119–B149). Hydrogens were added using standard geometries, and their positions were optimized using the molecular mechanics program AMBER.⁴⁴ All atom pairs were considered in the calculation of the nonbonded interactions, and a dielectric constant ($\epsilon (=r_{ij})$) was used. When Glu-B138 was mutated to Lys, the rotamer producing the lowest nonbonded energy was chosen, and a short optimization run restraining all backbone atoms to their initial coordinates allowed readjustment of covalent bonds and van der Waals contacts without changing the overall conformation of the protein. For the R172A mutant, all the side chain atoms in Arg-A172 beyond the C_β atom were replaced with a hydrogen. Since the region of interest is directed toward the solvent, a spherical "drop" of about 370 TIP3P water molecules, generated from a Monte Carlo simulation,⁴⁵ was added to each of the previous models centered on the C_α atom of residue B138 (CAP option in AMBER).

c. Molecular Mechanics and Molecular Dynamics Calculations. All the molecular systems that were studied were gradually refined in AMBER using a cutoff of 10.0 Å and a distance-dependent dielectric constant ($\epsilon = r_{ij}$). First, only the water molecules were allowed to reorient, and then the water molecules and all protein residues except those used for capping were allowed to relax, although the protein backbone was initially restrained to the crystallographic position with a force constant of 2 kcal mol⁻¹ Å⁻². In each case, 100 steps of steepest descent were followed by conjugate gradient energy minimization until the root-mean-square (rms) value of the potential energy gradient was <0.01 kcal mol⁻¹ Å⁻¹. The final coordinate sets were used as input for the subsequent molecular dynamics (MD) simulation under the same dielectric conditions. The use of the SHAKE algorithm to constrain all bond lengths to their equilibrium values allowed an integration time step of 2 fs to be employed. In a 5 ps heating phase, the temperature was increased from 0.2 to 298 K, and the velocities were reassigned at each new temperature according to a Maxwell–Boltzmann distribution. During the equilibration phase, positional restraints were applied to both the ligand and the protein C_α atoms, 2 kcal mol⁻¹ Å⁻² for the first 300 ps and 1 kcal mol⁻¹ Å⁻² for the following 240 ps, after which the ligand was completely free but the protein C_α atoms were still restrained for a further 720 ps. For the next 400 ps, the C_α restraints were removed for the β7–β8 loop and the β strands containing the catalytic Asp residues, and for the remaining 1600 ps, the whole system was free to move except for the capping residues which were positionally restrained with a force constant of 1 kcal mol⁻¹ Å⁻². The list of nonbonded pairs was updated every 25 steps, and coordinates were saved every 2 ps for visualization and every 80 ps for further analysis focusing on the last 2 ns of the trajectory. In this latter case, the coordinates from each MD snapshot were refined following a short energy minimization protocol that maintained the same set of positional restraints used in the corresponding MD simulation period. Molecular mechanics interaction energies between different parts of the system were calculated using the ANAL module of AMBER, and electrostatics were computed by means of the continuum method described below.

d. Parametrization and Conformational Search of TSAO-m³T. Two models of TSAO-m³T, one anti and one syn, were built in Insight II⁴⁶ using standard bond lengths and angles. Their geometries were optimized using the ab initio quantum chemistry program Gaussian⁴⁷ and the 3-21G* basis set. A common set of atom-centered RHF 6-31G**/3-21G* charges for TSAO-m³T (Table 1 of the Supporting Information) was then obtained by using the RESP methodology⁴⁸ and assigning equal weights to both conformations. Covalent and nonbonded parameters were derived, by analogy or through interpolation, from those already present in the AMBER force field.⁴⁹ The phase space for TSAO-m³T was sampled by using a combination of quenched MD and energy minimization

techniques, as previously described for other ligands.^{43,50} Each initial conformation was heated from 6 to 600 ± 10 K in 10 ps using classical MD and a time step of 0.5 fs. After a further 20 ps of equilibration, it was slowly cooled back to the initial temperature and energy minimized by using 100 steps of the steepest descent method and then switching over to conjugate gradient until the rms gradient was less than 0.01 kcal mol⁻¹ Å⁻¹. Each resulting structure was subjected to the same simulated annealing protocol, and the whole procedure was repeated 50 times. Ring puckering was used as a means of distinguishing among conformational families, and one member of each family was then used as a separate molecule for the automated docking procedure.

e. Docking Studies and Complex Refinement. The genetic algorithm⁵¹ implemented in AutoDock⁵² was used to generate different RT-bound TSAO-m³T conformers by randomly changing the torsion angles and overall orientation of the molecule. Changes in ring puckering were incorporated via inclusion of the different conformers found previously. A volume for exploration was defined in the shape of a three-dimensional cubic grid⁵³ with a spacing of 0.3 Å that enclosed the surroundings of Glu-B138, the NNRTI binding pocket, and a long portion of the intersubunit cleft. At each grid point, the receptor's atomic affinity potentials for carbon, oxygen, nitrogen, sulfur, and hydrogen atoms were precalculated for rapid intra- and intermolecular energy evaluation of each docked configuration. The buried Si atoms in TSAO-m³T were assimilated to C atoms. The NNRTI nevirapine,⁴ its 9-nitro derivative 1051U91,⁵⁴ the bis(heteroaryl)piperazine U90152,⁵⁵ and α -anilino phenyl acetamide (α -APA)⁴ were used as controls of program performance.

After addition of a cap of water molecules as described above for the free enzyme, the selected complex was gradually refined using AMBER. In a first stage, only the hydrogen atoms of the water molecules were allowed to reorient in the field of the complex. Then the geometry of the inhibitor was optimized while the atoms of both the protein and the water molecule were held fixed. Finally, the whole complex was energy minimized, and an MD trajectory was simulated as explained above, collecting data from the last 2 ns for further analysis.

f. Continuum Electrostatics Calculations. Finite difference solutions to the linearized Poisson–Boltzmann equation, as implemented in the DelPhi module of Insight II, were used to calculate MEPs and electrostatic free energies. For MEP calculations on TSAO-m³T and the putative RT binding site, cubic grids with a resolution of 1.0 Å were centered on the molecular systems considered following removal of the explicit water molecules, and the charges were distributed onto the grid points. AMBER charges and radii were used. Solvent-accessible surfaces, calculated with a spherical probe with a radius of 1.4 Å, defined the solute boundaries, and a minimum separation of 15 Å was left between any solute atom and the borders of the box. The potentials at the grid points delimiting the box were calculated analytically by treating each charge atom as a Debye–Hückel sphere. The interior of both the protein and the ligand was considered a low-dielectric medium ($\epsilon = 4$), whereas the surrounding solvent was treated as a high-dielectric medium ($\epsilon = 80$) with an ionic strength of 0.145 M. Two focusing calculations⁵⁶ followed, for which progressively smaller (borders of 12 and 9 Å) and finer grids (0.75 and 0.5 Å spacing) were used, together with new boundary potentials linearly interpolated from those calculated in the previous run.

Electrostatic free energies were calculated similarly using identical cubic grids of 0.75 Å resolution and no focusing. We have previously shown that focusing in this case does not lead to a significant improvement in the overall results.⁵⁷ For the processes of dimer formation and ligand association, the change in electrostatic free energy upon binding (ΔG_{ele}) was computed by considering two stages, as described in detail elsewhere.^{43,57} To calculate the electrostatic contribution to the desolvation of just one protein residue, charges were assigned only to the atoms belonging to that residue in both the protein and the protein–ligand complex.

g. Structure-Based Modification of TSAO-T. The Insight II⁴⁶ implementation of the LUDI program⁵⁸ was used to append suitable fragments onto the N3 atom of the thymine of the prototype TSAO-T, as found in the proposed complex of TSAO-m³T with wild-type RT. Interaction sites were calculated within a radius of 10 Å. The fit was achieved with a maximum rms deviation of 0.6 Å using the default fragment database.

B. Chemical Procedures. Microanalyses were carried out with a Heraeus CHN-O-RAPID instrument. Electrospray mass spectra were recorded on a quadrupole mass spectrometer equipped with an electrospray source (Hewlett-Packard, LC/MS HP 1100). ¹H and ¹³C NMR spectra were recorded on a Varian XL-300 spectrometer operating at 299 MHz for ¹H and 75 MHz for ¹³C using acetone-*d*₆ or CDCl₃ as the solvent at 30 °C with TMS as the internal standard.

One-dimensional ¹H and ¹³C spectra were obtained using standard conditions. Homonuclear two-dimensional spectra (COSY) were acquired in the phase-sensitive mode. Data were collected in a 2048 × 512 matrix with a spectral width of 3461 Hz and 1.2 s of relaxation delay and then processed in a 2048 × 1024 matrix. Two-dimensional inverse proton-detected heteronuclear one-bond shift correlation spectra were obtained using the pulsed field gradient HSQC pulse sequence. Data were collected in a 2048 × 512 matrix with a spectral width of 3460 Hz in the proton domain and 22 500 Hz in the carbon domain, and processed in a 2048 × 1024 matrix. The experiment was optimized for one bond heteronuclear coupling constant of 150 Hz. Two-dimensional inverse proton-detected heteronuclear long-range shift correlation spectra were obtained using the pulsed field gradient HMBC pulse sequence. The HMBC experiment was carried out under the same conditions that were used for the HSQC experiment and optimized for long-range coupling constants of 7 Hz.

Analytical TLC was performed on silica gel 60 F₂₅₄ (Merck) precoated plates (0.2 mm). Separations on silica gel were performed by preparative centrifugal circular thin-layer chromatography (CCTLC) on a chromatotron [Kiesegel 60 PF₂₅₄ gipshaltig (Merck); layer thickness of 1 mm; flow rate of 5 mL/min]. Flash column chromatography was performed with silica gel 60 (230–400 mesh) (Merck). Preparative chromatographic purifications were performed on 20 cm × 20 cm glass plates coated with a 2 mm layer of silica gel PF₂₅₄ (Merck).

{1-[2',5'-Bis-*O*-(*tert*-butyldimethylsilyl)- β -D-ribofuranosyl]-4-thiothymine}-3'-spiro-5'-(4'-amino-1'',2''-oxathiole-2'',2''-dioxide) (**2**). To a solution of TSAO-T²⁹ (0.2 g, 0.34 mmol) in dry toluene (10 mL) was added the Lawesson's reagent (0.17 g, 0.41 mmol). The reaction mixture was refluxed for 3 h and then concentrated to dryness. The residue thus obtained was purified by preparative CCTLC on the chromatotron (2:1 hexane/ethyl acetate) to give **2** (0.125 g, 60%) as an amorphous solid: ¹H NMR [(CD₃)₂CO] δ 2.05 (d, 3H, *J* = 1.3 Hz, CH₃-5), 4.06 (m, 1H, *J*_{4',5'a} = 3.8 Hz, *J*_{5'a,5'b} = 7.6 Hz, H-5'a), 4.10 (m, 1H, *J*_{4',5'b} = 3.4 Hz, H-5'b), 4.34 (dd, 1H, H-4'), 4.71 (d, 1H, *J*_{1',2'} = 8.1 Hz, H-2'), 5.99 (d, 1H, H-1'), 6.47 (bs, 2H, NH₂), 7.56 (d, 1H, H-6), 11.65 (bs, 1H, NH); ¹³C NMR [(CD₃)₂CO] δ 17.23 (CH₃-5), 18.39, 18.95 [(CH₃)₃-C-Si], 25.72, 26.34 [(CH₃)₃-C-Si], 63.02 (C-5'), 75.35 (C-2'), 85.38, 87.65 (C-4', C-1'), 87.68 (C-3'), 92.31 (C-3'), 120.05 (C-5), 132.46 (C-6), 148.78 (C-4'), 152.03 (C-2), 192.33 (C-4). Anal. (C₂₄H₄₃N₃O₇S₂-Si₂) C, H, N.

{1-[2',5'-Bis-*O*-(*tert*-butyldimethylsilyl)- β -D-ribofuranosyl]-3,4-dihydro-5-methyl-2-pyrimidone}-3'-spiro-5'-(4'-amino-1'',2''-oxathiole-2'',2''-dioxide) and {1-[2',5'-Bis-*O*-(*tert*-butyldimethylsilyl)- β -D-ribofuranosyl]-3,6-dihydro-5-methyl-2-pyrimidone}-3'-spiro-5'-(4'-amino-1'',2''-oxathiole-2'',2''-dioxide) (**3** and **4**, respectively). A solution of thio derivative **2** (0.1 g, 0.17 mmol) and NiCl₂·6H₂O (0.33 g, 1.37 mmol) in a MeOH/THF mixture (1:1.4, 2.4 mL) was treated, at 0 °C, with NaBH₄ (0.31 g, 8.25 mmol). After being stirred at room temperature for 30 min, the reaction mixture was filtered through Celite and the solvents were evaporated to dryness. The resulting residue was dissolved in CH₂Cl₂ (20 mL) and washed with NaHCO₃ (2 × 10 mL), a saturated solution of EDTA (10 mL), and H₂O (10 mL). The organic layer

was dried (Na_2SO_4) and evaporated to give a residue which was purified first by CCTLC on the chromatotron (3:1 hexane/ethyl acetate) and then by preparative TLC (3:2 hexane/ethyl acetate). The faster moving band afforded 0.020 g (20%) of **4** as a white amorphous solid: ^1H NMR $[(\text{CD}_3)_2\text{CO}] \delta$ 1.67 (d, 3H, $J = 1.1$ Hz, CH_3 -5), 3.80–4.02 (m, 4H, 2H-5', CH_2 -6), 4.10 (dd, 1H, $J_{4,5'a} = 4.1$ Hz, $J_{4,5'b} = 3.1$ Hz, H-4'), 4.67 (d, 1H, $J_{1,2'} = 7.9$ Hz, H-2'), 5.64 (s, 1H, H-3'), 5.74 (d, 1H, H-1'), 5.93 (m, 1H, H-4), 6.48 (bs, 2H, NH_2), 7.42 (m, 1H, NH); ^{13}C NMR $[(\text{CD}_3)_2\text{CO}] \delta$ 16.99 (CH_3 -5), 18.64, 18.95 $[(\text{CH}_3)_3\text{-C-Si}]$, 25.95, 26.40 $[(\text{CH}_3)_3\text{-C-Si}]$, 46.90 (CH_2 -6), 63.19 (C-5'), 71.95 (C-2'), 83.67 (C-4'), 89.02 (C-1'), 91.31 (C-3'), 92.22 (C-3'), 106.14 (C-5), 120.72 (C-4), 153.58 (C-4'), 154.10 (C-2); MS (ES+) *m/e* 598.3 (M + Na^+). Anal. ($\text{C}_{24}\text{H}_{45}\text{N}_3\text{O}_7\text{SSi}_2$) C, H, N.

The slowest moving band gave 0.024 g (25%) of **3** as a white amorphous solid: ^1H NMR $[(\text{CD}_3)_2\text{CO}] \delta$ 1.69 (d, 3H, $J = 0.5$ Hz, CH_3 -5), 3.82 (m, 1H, $J_{4a,4b} = 15.1$ Hz, $J_{4a,\text{NH}} = 1.3$ Hz, H-4a), 3.88 (m, 1H, $J_{4b,\text{NH}} = 2.6$ Hz, H-4b), 3.94 (m, 1H, $J_{4,5'a} = 4.4$ Hz, $J_{5'a,5'b} = 12.0$ Hz, H-5'a), 4.03 (m, 1H, $J_{4,5'b} = 3.1$ Hz, H-5'b), 4.09 (dd, 1H, H-4'), 4.60 (d, 1H, $J_{1,2'} = 7.8$ Hz, H-2'), 5.59 (d, 1H, H-1'), 5.62 (s, 1H, H-3'), 6.15 (d, 1H, H-6), 6.19 (dd, 1H, NH), 6.51 (bs, 2H, NH_2); ^{13}C NMR $[(\text{CD}_3)_2\text{CO}] \delta$ 16.54 (CH_3 -5), 18.43, 18.75 $[(\text{CH}_3)_3\text{-C-Si}]$, 25.76, 26.08 $[(\text{CH}_3)_3\text{-C-Si}]$, 45.52 (C-4), 62.89 (C-5'), 75.95 (C-2'), 83.44 (C-4'), 89.78 (C-1'), 90.71 (C-3'), 92.31 (C-3'), 110.82 (C-5), 121.76 (C-6), 153.77 (C-2), 157.57 (C-4'). Anal. ($\text{C}_{24}\text{H}_{45}\text{N}_3\text{O}_7\text{SSi}_2$) C, H, N.

{1-[2',5'-Bis-*O*-(*tert*-butyldimethylsilyl)- β -D-ribofuranosyl]-3-*N*-(3-hydroxypropyl)thymine}-3'-spiro-5''-(4''-amino-1'',2''-oxathiole-2'',2''-dioxide) (5). To a solution of TSAO-T²⁹ (0.20 g, 0.34 mmol) in dry acetone (6 mL) were added dry K_2CO_3 (0.05 g, 0.37 mmol) and 3-bromopropanol (0.09 mL, 1.02 mmol). The reaction mixture was refluxed for 6 h and then concentrated to dryness. The residue was dissolved in ethyl acetate (20 mL) and washed with brine (2×20 mL). The organic layer was dried (Na_2SO_4), filtered, and evaporated to dryness. The residue was purified by flash column chromatography (2:1 hexane/ethyl acetate) to afford **5** (0.17 g, 78%) as a white amorphous solid: ^1H NMR $[(\text{CD}_3)_2\text{CO}] \delta$ 1.78 (m, 2H, CH_2), 1.94 (s, 3H, CH_3 -5), 3.52 (m, 3H, CH_2OH , OH), 4.05 (m, 4H, H-5', CH_2N), 4.33 (t, 1H, $J_{4,5'} = 3.6$ Hz, H-4'), 4.68 (d, 1H, H-2'), 5.75 (s, 1H, H-3'), 6.07 (d, 1H, $J_{1,2'} = 8.1$ Hz, H-1'), 6.42 (bs, 2H, NH_2 -4''), 7.50 (s, 1H, H-6); ^{13}C NMR $(\text{CD}_3\text{Cl}_3) \delta$ 12.87 (CH_3 -5), 30.38 (CH_2), 38.20 (CH_2N), 58.56 (CH_2OH), 62.11 (C-5'), 74.72 (C-2'), 83.60, 87.70 (C-3'', C-4'), 92.15 (C-3'), 93.25 (C-1'), 110.99 (C-5), 134.11 (C-6), 150.52, 151.25 (C-2, C-4''), 163.85 (C-4). Anal. ($\text{C}_{27}\text{H}_{49}\text{N}_3\text{O}_9\text{SSi}_2$) C, H, N.

C. Biological Methods. a. Construction of the Mutant Enzymes. The E138K mutant RT enzyme was constructed as described previously.⁵⁹ The K172A mutant RT enzyme used in this study was derived from the RT sequence cloned in pKRT2His.⁶⁰ Site-directed mutagenesis was performed using the QuikChange site-directed mutagenesis kit from Stratagene. The K172A mutagenesis primer (sense, 5'-GCATGACAAAATCTTAGAGCCTTTCGCGAAACAAAATCCAG-3') was ordered PAGE-purified from Amersham Pharmacia Biotech. When the lysine was changed to alanine, a *Dra*I restriction site was abolished which made it possible to determine the presence of the mutation by restriction analysis. The K172A mutant RT enzyme used for analysis of the NNRTI resistance profile was an *Escherichia coli* lysate prepared as described previously.⁶⁰

b. Activity Assay for Test Compounds against HIV-1 in Cell Cultures. CEM cells were obtained from the American Type Cell Culture Collection (Manassas, VA). MT-4 cells were provided by N. Yamamoto (Tokyo Medical School and Dental University School of Medicine, Tokyo, Japan). CEM and MT-4 cells were suspended at a density of approximately 200000–300000 cells/mL of culture medium and infected with wild-type HIV-1 (III_B). Then, 100 μL of the infected cell suspensions was added to 200 μL microtiter plate wells containing 100 μL of an appropriate dilution of the test compounds. After incubation for 4 (CEM) or 5 days (MT-4) at 37 °C, the cell cultures were microscopically examined for syncytium formation (CEM) or counted by trypan blue dye exclusion (MT-4).

The EC₅₀ (50% effective concentration) was determined as the compound concentration required to inhibit syncytium formation (CEM) or to reduce cell viability (MT-4) by 50%.

c. RT Enzyme Assay. For determination of the 50% inhibitory concentration (IC₅₀) of the test compounds, the RT assay was performed as described previously.¹³ A fixed concentration of the labeled substrate [2,8-³H]dGTP (specific radioactivity of 3.6 Ci/mmol) (5.6 μM , 1 μCi ; Amersham Pharmacia Biotech) and a fixed concentration of the template-primer poly(C)·oligo(dG)_{12–18} (0.1 mM; Amersham Pharmacia Biotech) were used. The IC₅₀ for each test compound was determined as the compound concentration that inhibited recombinant RT activity by 50%.

Acknowledgment. We thank Lizette van Berckelaer and Ann Absillis for excellent technical assistance. Fellowships to E.L. and C.P. (Spanish Ministerio de Educación y Cultura) are gratefully acknowledged. The University of Alcalá Computing Centre granted a generous allowance of computer time on a SGI Power Challenge server. This research has been financed by the Spanish CICYT (Project SAF2000-0153-C02 to M.-J.C. and F.G.), the Geconcerteerde Onderzoeksacties (GOA) (Krediet 00/12) of the "Vlaamse Gemeenschap", and the European Commission (Project QLRT-1999-30291).

Supporting Information Available: A table containing atomic RESP charges for TSAO-m³T and four figures showing buried solvent-accessible surface area of individual residues from both the p66 and p51 subunits of HIV-1 RT upon dimerization (Figure 1), van der Waals and electrostatic contributions to the dimerization energy of HIV-1 RT of residues comprising or near the $\beta 7$ – $\beta 8$ loop (Figure 2), time evolution of the rmsd from the corresponding refined initial structure along the MD trajectories for wild-type RT, with and without bound TSAO-m³T (Figure 3), and an MEP difference map calculated between wild-type and R172A RT enzymes in aqueous solution at physiological pH (Figure 4). This material is available free of charge via the Internet at <http://pubs.acs.org>.

References

- Basu, A.; Basu, S.; Modak, M. J. Structure–activity analyses of HIV-1 reverse transcriptase. *Biochem. Biophys. Res. Commun.* **1992**, *183*, 1131–1138.
- (a) Rodgers, D. W.; Gambin, S. J.; Harris, B. A.; Ray, S.; Culp, J. S.; Hellmig, B.; Woolf, D. J.; Debouck, C.; Harrison, S. C. The structure of unliganded reverse transcriptase from the human immunodeficiency virus type 1. *Proc. Natl. Acad. Sci. U.S.A.* **1995**, *92*, 1222–1226. (b) Hsiou, Y.; Ding, J.; Das, K.; Clark, A. D., Jr.; Hughes, S. H.; Arnold, E. Structure of unliganded HIV-1 reverse transcriptase at 2.7 Å resolution: implications of conformational changes for polymerization and inhibition mechanisms. *Structure* **1996**, *4*, 853–860.
- (a) Jacobo-Molina, A.; Ding, J.; Nanni, R. G.; Clark, A. D., Jr.; Lu, X.; Tantillo, C.; Williams, R. L.; Kamer, G.; Ferris, A. L.; Clark, P.; Hizi, A.; Hughes, S. H.; Arnold, E. Crystal structure of human immunodeficiency virus type 1 reverse transcriptase complexed with double-stranded DNA at 3.0 Å resolution shows bent DNA. *Proc. Natl. Acad. Sci. U.S.A.* **1993**, *90*, 6320–6324. (b) Huang, H.; Chopra, R.; Verdine, G. L.; Harrison, S. C. Structure of a covalently trapped catalytic complex of HIV-1 reverse transcriptase: implications for drug resistance. *Science* **1998**, *282*, 1669–1675.
- Ren, J.; Esnouf, R.; Garman, E.; Somers, D.; Ross, C.; Kirby, I.; Keeling, J.; Darby, G.; Jones, Y.; Stuart, D.; Stammers, D. High resolution structures of HIV-1 RT from four RT-inhibitor complexes. *Nat. Struct. Biol.* **1995**, *2*, 293–302.
- Wang, J.; Smerdon, S. J.; Jager, J.; Kohlstaedt, L. A.; Rice, P. A.; Friedman, J. M.; Steitz, T. A. Structural basis of asymmetry in the human immunodeficiency virus type 1 reverse transcriptase heterodimer. *Proc. Natl. Acad. Sci. U.S.A.* **1994**, *91*, 7242–7246.
- Amacker, M.; Hübscher, U. Chimeric HIV-1 and feline immunodeficiency virus reverse transcriptases: critical role of the p51 subunit in the structural integrity of heterodimeric lentiviral DNA polymerases. *J. Mol. Biol.* **1998**, *278*, 757–765.

- (7) Harris, D.; Lee, R.; Misra, H. S.; Pandey, P. K.; Pandey, V. N. The p51 subunit of human immunodeficiency virus type 1 reverse transcriptase is essential in loading the p66 subunit on the template primer. *Biochemistry* **1998**, *37*, 5903–5908.
- (8) Divita, G.; Restle, T.; Goody, R. S. Characterization of the dimerization process of HIV-1 reverse transcriptase heterodimer using intrinsic protein fluorescence. *FEBS Lett.* **1993**, *324*, 153–158.
- (9) Divita, G.; Rittinger, K.; Geourjon, C.; Deléage, G.; Goody, R. S. Dimerization kinetics of HIV-1 and HIV-2 reverse transcriptase: a two step process. *J. Mol. Biol.* **1995**, *245*, 508–521.
- (10) (a) De Clercq, E. Toward improved anti-HIV chemotherapy: therapeutic strategies for intervention with HIV infections. *J. Med. Chem.* **1995**, *38*, 2491–2517. (b) Esnouf, R.; Ren, J.; Ross, C.; Jones, Y.; Stammers, D.; Stuart, D. Mechanism of inhibition of HIV-1 reverse transcriptase by non-nucleoside inhibitors. *Nat. Struct. Biol.* **1995**, *2*, 303–308.
- (11) Balzarini, J. Suppression of resistance to drugs targeted to human immunodeficiency virus reverse transcriptase by combination therapy. *Biochem. Pharmacol.* **1999**, *58*, 1–27.
- (12) Schinazi, R. F.; Larder, B. A.; Mellors, J. W. Mutations in retroviral genes associated with drug resistance: 2000–2001 update. *Int. Antiviral News* **2000**, *8*, 65–91.
- (13) Balzarini, J.; Pérez-Pérez, M. J.; San-Félix, A.; Schols, D.; Perno, C. F.; Vandamme, A. M.; Camarasa, M. J.; De Clercq, E. 2',5'-bis-*O*-(*tert*-butyldimethylsilyl)-3'-spiro-5''-(4''-amino-1'',2''-oxathiole-2'',2'-dioxide)pyrimidine (TSAO) nucleoside analogues: highly selective inhibitors of human immunodeficiency virus type 1 that are targeted at the viral reverse transcriptase. *Proc. Natl. Acad. Sci. U.S.A.* **1992**, *89*, 4392–4396.
- (14) Balzarini, J.; Pérez-Pérez, M. J.; San-Félix, A.; Camarasa, M. J.; Bathurst, I. C.; Barr, P. J.; De Clercq, E. Kinetics of inhibition of human immunodeficiency virus type 1 (HIV-1) reverse transcriptase by the novel HIV-1-specific nucleoside analogue [2',5'-bis-*O*-(*tert*-butyldimethylsilyl)-β-D-ribofuranosyl]-3'-spiro-5''-(4''-amino-1'',2''-oxathiole-2'',2'-dioxide)thymine (TSAO-T). *J. Biol. Chem.* **1992**, *267*, 11831–11838.
- (15) (a) Jonckheere, H.; Taymans, J. M.; Balzarini, J.; Velázquez, S.; Camarasa, M. J.; Desmyter, J.; De Clercq, E.; Anne, J. Resistance of HIV-1 reverse transcriptase against [2',5'-bis-*O*-(*tert*-butyldimethylsilyl)-3'-spiro-5''-(4''-amino-1'',2''-oxathiole-2'',2'-dioxide)] (TSAO) derivatives is determined by the mutation Glu138→Lys on the p51 subunit. *J. Biol. Chem.* **1994**, *269*, 25255–25258. (b) Balzarini, J.; Velázquez, S.; San-Félix, A.; Karlsson, A.; Pérez-Pérez, M. J.; Camarasa, M. J.; De Clercq, E. Human immunodeficiency virus type 1-specific [2',5'-bis-*O*-(*tert*-butyldimethylsilyl)-β-D-ribofuranosyl]-3'-spiro-5''-(4''-amino-1'',2''-oxathiole-2'',2'-dioxide)purine analogues show a resistance spectrum that is different from that of the human immunodeficiency virus type 1-specific non-nucleoside analogues. *Mol. Pharmacol.* **1993**, *43*, 109–114.
- (16) Balzarini, J.; Karlsson, A.; Vandamme, A. M.; Pérez-Pérez, M. J.; Zhang, H.; Vrang, L.; Oberg, B.; Backbro, K.; Unge, T.; San-Félix, A.; Velázquez, S.; Camarasa, M. J.; De Clercq, E. Human immunodeficiency virus type 1 (HIV-1) strains selected for resistance against the HIV-1-specific [2',5'-bis-*O*-(*tert*-butyldimethylsilyl)-3'-spiro-5''-(4''-amino-1'',2''-oxathiole-2'',2'-dioxide)]-β-D-pentofuranosyl (TSAO) nucleoside analogues retain sensitivity to HIV-1-specific nonnucleoside inhibitors. *Proc. Natl. Acad. Sci. U.S.A.* **1993**, *90*, 6952–6956.
- (17) Sluis-Cremer, N.; Dmitrienko, G. I.; Balzarini, J.; Camarasa, M. J.; Parniak, M. A. Human immunodeficiency virus type 1 reverse transcriptase dimer destabilization by 1-[spiro[4''-amino-2'',2''-dioxo-1'',2''-oxathiole-5'',3'-]-2',5'-bis-*O*-(*tert*-butyldimethylsilyl)-β-D-ribofuranosyl]]-3-ethylthymine. *Biochemistry* **2000**, *39*, 1427–1433.
- (18) Harris, D.; Lee, R.; Misra, H. S.; Pandey, P. K.; Pandey, V. N. The p51 subunit of human immunodeficiency virus type 1 reverse transcriptase is essential in loading the p66 subunit on the template primer. *Biochemistry* **1998**, *37*, 5903–5908.
- (19) Camarasa, M. J.; San-Félix, A.; Pérez-Pérez, M. J.; Velázquez, S.; Alvarez, R.; Chamorro, C.; Jimeno, M.-L.; Pérez, C.; Gago, F.; De Clercq, E.; Balzarini, J. HIV-1 specific reverse transcriptase inhibitors: why are TSAO-nucleosides so unique?. *J. Carbohydr. Chem.* **2000**, *19*, 451–469.
- (20) Alvarez, R.; Jimeno, M. L.; Gago, F.; Balzarini, J.; Pérez-Pérez, M. J.; Camarasa, M. J. Novel 3'-spiro nucleoside analogues of TSAO-T. Part II. A comparative study based on NMR conformational analysis in solution and theoretical calculations. *Antiviral Chem. Chemother.* **1998**, *9*, 333–340.
- (21) Ingate, S.; Pérez-Pérez, M. J.; De Clercq, E.; Balzarini, J.; Camarasa, M. J. Synthesis and anti-HIV-1 activity of novel TSAO-T derivatives modified at the 2'- and 5'-positions of the sugar moiety. *Antiviral Res.* **1995**, *27*, 281–299.
- (22) Velázquez, S.; Alvarez, R.; Pérez, C.; Gago, F.; De Clercq, E.; Balzarini, J.; Camarasa, M. J. Regiospecific synthesis and anti-human immunodeficiency virus activity of novel 5-substituted *N*-alkylcarbamoyl and *N,N*-dialkylcarbamoyl 1,2,3-triazole-TSAO analogues. *Antiviral Chem. Chemother.* **1998**, *9*, 481–489.
- (23) Velázquez, S.; Chamorro, C.; Pérez-Pérez, M. J.; Alvarez, R.; Jimeno, M.-L.; Martín-Domenech, A.; Pérez, C.; Gago, F.; de Clercq, E.; Balzarini, J.; San-Félix, A.; Camarasa, M. J. Abasic analogues of TSAO-T as the first sugar derivatives that specifically inhibit HIV-1 reverse transcriptase. *J. Med. Chem.* **1998**, *41*, 4636–4647.
- (24) (a) Velázquez, S.; Tuñón, V.; Jimeno, M. L.; Pérez-Pérez, M. J.; San-Félix, A.; Chamorro, C.; Lobatón, E.; Esteban-Gamboa, A.; De Clercq, E.; Balzarini, J.; Camarasa, M. J. Novel series of [ddN]-[TSAO-T] heterodimers as potential bi-functional inhibitors of HIV-1 RT. Studies in the linker and ddN region. *Nucleosides Nucleotides* **1999**, *18*, 1029–1030. (b) Velázquez, S.; Tuñón, V.; Jimeno, M. L.; Chamorro, C.; De Clercq, E.; Balzarini, J.; Camarasa, M. J. Potential multifunctional inhibitors of HIV-1 reverse transcriptase. Novel [AZT]-[TSAO-T] and [d4T]-[TSAO-T] heterodimers modified in the linker and in the dideoxynucleoside region. *J. Med. Chem.* **1999**, *42*, 5188–5196.
- (25) Divita, G.; Rittinger, K.; Restle, T.; Immendorfer, U.; Goody, R. S. Conformational stability of dimeric HIV-1 and HIV-2 reverse transcriptases. *Biochemistry* **1995**, *34*, 16337–16346.
- (26) Clackson, T.; Wells, J. A. A hot spot of binding energy in a hormone-receptor interface. *Science* **1995**, *267*, 383–386.
- (27) Luengo, S.; Rodríguez-Barrios, F.; Jimeno, M. L.; Camarasa, M. J.; Gago, F. Unpublished results.
- (28) IUPAC-IUB Joint Commission on Biochemical Nomenclature. Abbreviations and Symbols for the Description of Conformations of Polynucleotide Chains. *Eur. J. Biochem.* **1983**, *131*, 9–15.
- (29) Pérez-Pérez, M. J.; San-Félix, A.; Balzarini, J.; De Clercq, E.; Camarasa, M. J. TSAO-analogues. Stereospecific synthesis and anti-HIV-1 activity of 1-[2',5'-bis-*O*-(*tert*-butyldimethylsilyl)-β-D-ribofuranosyl]-3'-spiro-5''-(4''-amino-1'',2''-oxathiole-2'',2'-dioxide) pyrimidine and pyrimidine-modified nucleosides. *J. Med. Chem.* **1992**, *35*, 2988–2995.
- (30) Pelemans, H.; Aertsen, A.; van Laethem, K.; Vandamme, A.-M.; De Clercq, E.; Pérez-Pérez, M. J.; San-Félix, A.; Velázquez, S.; Camarasa, M.-J.; Balzarini, J. Site-directed mutagenesis of human immunodeficiency virus type 1 reverse transcriptase at amino acid position 138. *Virology*, in press.
- (31) (a) Guzic, F. S.; Wasmund, L. M. An improved method for the preparation of desoxopeptides: Reduction of endothiopyptides. *Tetrahedron Lett.* **1990**, *31*, 23–26. (b) Khurana, J. M.; Gogia, A. Synthetically useful reactions with nickel boride. A review. *Org. Prep. Proced. Int.* **1997**, *29*, 1–32.
- (32) (a) Fox, J. J.; Praag, D. V. Pyrimidine Nucleosides. V. 2-Oxo-hexahydropyrimidines and their nucleosides. *J. Am. Chem. Soc.* **1960**, *82*, 486–489. (b) Wightman, R.; Holy, A. Nucleic Acid Components and their analogues. CLIX. Synthesis of some 2-pyrimidone nucleosides. *Collect. Czech. Chem. Commun.* **1973**, *38*, 1381–1396.
- (33) (a) Scheibye, S.; Pedersen, B. S.; Lawesson, S.-O. Studies on organophosphorus compounds. XXI. The dimer of *p*-methoxyphenylthiophosphine sulfide as thiation reagent. A new route to thiocarboxamides. *Bull. Soc. Chim. Belg.* **1978**, *87*, 229–238. (b) Palomino, E.; Meltsner, B. R.; Kessel, D.; Horwitz, J. P. Synthesis and in vitro evaluation of some modified 4-thiopyrimidine nucleosides for prevention or reversal of AIDS-associated neurological disorders. *J. Med. Chem.* **1990**, *33*, 258–263. (c) Czernecki, S.; Le Diguarher, T.; Valéry, J. M. Synthesis and anti-HIV-1 activity of base modified analogues of 3'-azido-2',3'-dideoxythymidine (AZT). *Nucleosides Nucleotides* **1993**, *12*, 369–380.
- (34) Everby, M. R.; Oldroyd, A. C.; Waigh, R. D. Synthesis of 4,5-dihydro-1*H*-imidazoles from 1,5-dihydro-2*H*-imidazoles using "nickel boride". *Heterocycles* **1986**, *24*, 2871–2877.
- (35) Arion, D.; Fletcher, R. S.; Borkow, G.; Camarasa, M. J.; Balzarini, J.; Dmitrienko, G. I.; Parniak, M. A. Differences in the inhibition of human immunodeficiency virus type 1 reverse transcriptase DNA polymerase activity by analogs of nevirapine and [2',5'-bis-*O*-(*tert*-butyldimethylsilyl)-3'-spiro-5''-(4''-amino-1'',2''-oxathiole-2'',2'-dioxide)] (TSAO). *Mol. Pharmacol.* **1996**, *50*, 1057–1064.
- (36) Esnouf, R.; Stuart, D. Unpublished results.
- (37) Misra, H. S.; Pandey, P. K.; Pandey, V. N. An enzymatically active chimeric HIV-1 reverse transcriptase (RT) with the RNase-H domain of murine leukemia virus RT exists as a monomer. *J. Biol. Chem.* **1998**, *273*, 9785–9789.
- (38) Esnouf, R.; Ren, J.; Ross, C.; Jones, Y.; Stammers, D.; Stuart, D. Mechanism of inhibition of HIV-1 reverse transcriptase by non-nucleoside inhibitors. *Nat. Struct. Biol.* **1995**, *2*, 302–308.
- (39) Balzarini, J.; Karlsson, A.; De Clercq, E. Human immunodeficiency virus type 1 drug-resistance patterns with different 1-[(2-hydroxyethoxy)methyl]-6-(phenylthio)thymine derivatives. *Mol. Pharmacol.* **1993**, *44*, 694–701.

- (40) Hubbard, S. J.; Thornton, J. M. *NACCESS*; Department of Biochemistry and Molecular Biology, University College London: London, 1993.
- (41) Lee, B.; Richards, F. M. The interpretation of protein structures: estimation of static accessibility. *J. Mol. Biol.* **1971**, *55*, 379–400.
- (42) Chothia, C. Hydrophobic bonding and accessible surface area in proteins. *Nature* **1974**, *248*, 338–339.
- (43) García-Nieto, R.; Pérez, C.; Gago, F. Automated docking and molecular dynamics simulations of nimesulide in the cyclooxygenase active site of human prostaglandin-endoperoxide synthase-2 (COX-2). *J. Comput.-Aided Mol. Des.* **2000**, *14*, 147–160.
- (44) Pearlman, D. A.; Case, D. A.; Caldwell, J.; Ross, W. S.; Cheatham, T. E.; Ferguson, D. M.; Seibel, G. L.; Singh, U. C.; Weiner, P.; Kollman, P. A. *AMBER*, version 4.1; Department of Pharmaceutical Chemistry, University of California: San Francisco, 1995.
- (45) Jorgensen, W. L.; Chandrasekhar, J.; Madura, J. D.; Impey, R. W.; Klein, M. L. Comparison of simple potential functions for simulating liquid water. *J. Chem. Phys.* **1983**, *79*, 926–935.
- (46) *Insight II*, version 98; Molecular Simulations Inc.: San Diego, 1998.
- (47) Frisch, M. J.; Trucks, G. W.; Schlegel, H. B.; Gill, P. M. W.; Johnson, B. G.; Robb, M. A.; Cheeseman, J. R.; Keith, T.; Petersson, G. A.; Montgomery, J. A.; Raghavachari, K.; Al-Laham, M. A.; Zakrzewski, V. G.; Ortiz, J. V.; Foresman, J. B.; Cioslowski, J.; Stefanov, B. B.; Nanayakkara, A.; Challacombe, M.; Peng, C. Y.; Ayala, P. Y.; Chen, W.; Wong, M. W.; Andres, J. L.; Replogle, E. S.; Gomperts, R.; Martin, R. L.; Fox, D. J.; Binkley, J. S.; Defrees, D. J.; Baker, J.; Stewart, J. P.; Head-Gordon, M.; Gonzalez, C.; Pople, J. A. *Gaussian 94*, revision E.1; Gaussian, Inc.: Pittsburgh, PA, 1995.
- (48) Bayly, C. I.; Cieplak, P.; Cornell, W. D.; Kollman, P. A. A well-behaved electrostatic potential based method using charge restraints for deriving atomic charges: the RESP model. *J. Phys. Chem.* **1993**, *97*, 10269–10280.
- (49) Cornell, W. D.; Cieplak, P.; Bayly, C. I.; Gould, I. R.; Merz, K. M.; Ferguson, D. M.; Spellmeyer, D. C.; Fox, T.; Caldwell, J. W.; Kollman, P. A. A second generation force field for the simulation of proteins, nucleic acids, and organic molecules. *J. Am. Chem. Soc.* **1995**, *117*, 5179–5197.
- (50) Ortiz, A. R.; Pisabarro, M. T.; Gago, F. Molecular model of the interaction of bee venom phospholipase A₂ with manoolide. *J. Med. Chem.* **1993**, *36*, 1866–1879.
- (51) Morris, G. M.; Goodsell, D. S.; Halliday, R. S.; Huey, R.; Hart, W. E.; Belew, R. K.; Olson, A. J. Automated docking using Lamarckian genetic algorithm and an empirical binding free energy function. *J. Comput. Chem.* **1998**, *19*, 1639–1662.
- (52) Morris, G. M.; Goodsell, D. S.; Huey, R.; Hart, W. E.; Halliday, S.; Belew, R.; Olson, A. J. *AutoDock: Automated docking of flexible ligands to receptors*, version 3.0; The Scripps Research Institute: La Jolla, CA, 1999.
- (53) Goodford, P. J. A computational procedure for determining energetically favorable binding sites on biologically important macromolecules. *J. Med. Chem.* **1985**, *28*, 849–857.
- (54) Ren, J.; Esnouf, R. M.; Hopkins, A. L.; Jones, E. Y.; Kirby, I.; Keeling, J.; Ross, C. K.; Larder, B. A.; Stuart, D. I.; Stammers, D. K. 3'-Azido-3'-deoxythymidine drug resistance mutations in HIV-1 reverse transcriptase can induce long range conformational changes. *Proc. Natl. Acad. Sci. U.S.A.* **1998**, *95*, 9518–9523.
- (55) Esnouf, R. M.; Ren, J.; Hopkins, A. L.; Ross, C. K.; Jones, E. Y.; Stammers, D. K.; Stuart, D. I. Unique features in the structure of the complex between HIV-1 reverse transcriptase and the bis-(heteroaryl)piperazine (BHAP) U-90152 explain resistance mutations for this nonnucleoside inhibitor. *Proc. Natl. Acad. Sci. U.S.A.* **1997**, *94*, 3984–3989.
- (56) Klapper, I.; Hagstrom, R.; Fine, R.; Sharp, K.; Honig, B. Focusing of electric fields in the active site of Cu-Zn superoxide dismutase: effects of ionic strength and amino-acid modification. *Proteins* **1986**, *1*, 47–59.
- (57) Pérez, C.; Ortiz, A. R.; Pastor, M.; Gago, F. Comparative binding energy analysis of HIV-1 protease inhibitors: incorporation of solvent effects and validation as a powerful tool in receptor-based drug design. *J. Med. Chem.* **1998**, *41*, 836–852.
- (58) (a) Böhm, H. J. The computer program LUDI: a new method for the de novo design of enzyme inhibitors. *J. Comput.-Aided Mol. Des.* **1992**, *6*, 61–78. (b) Böhm, H. J. LUDI: rule-based automatic design of new substituents for enzyme inhibitor leads. *J. Comput.-Aided Mol. Des.* **1992**, *6*, 593–606.
- (59) Balzarini, J.; Kleim, J.-P.; Riess, G.; Camarasa, M.-J.; De Clercq, E.; Karlsson, A. Sensitivity of (138 Glu → Lys) mutated human immunodeficiency virus type 1 (HIV-1) reverse transcriptase (RT) to HIV-1-specific RT inhibitors. *Biochem. Biophys. Res. Commun.* **1994**, *201*, 1305–1312.
- (60) Pelemans, H.; Esnouf, R. M.; Jonckheere, H.; De Clercq, E.; Balzarini, J. Mutational analysis of Tyr-318 within the non-nucleoside reverse transcriptase inhibitor binding pocket of human immunodeficiency virus type I reverse transcriptase. *J. Biol. Chem.* **1998**, *273*, 34234–34239.

JM001095I